Climatic Regulation of Vegetation Phenology in Protected Areas along Western South America

Carlos Lara, Gonzalo S Saldías, Bernard Cazelles, Marcelo M Rivadeneira, Richard Muñoz, Alexander Galán, Álvaro L Paredes, Pablo Fierro, Bernardo R Broitman

HAL Id: hal-03280255

https://hal.sorbonne-universite.fr/hal-03280255v1

Submitted on 7 Jul 2021

Climatic Regulation of Vegetation Phenology in Protected Areas along Western South America

Carlos Lara [1,2], Gonzalo S. Saldías [3,4,*], Bernard Cazelles [5,6], Marcelo M. Rivadeneira [7,8,9], Richard Muñoz [10], Alexander Galán [11], Álvaro L. Paredes [12], Pablo Fierro [13] and Bernardo R. Broitman [14]

1 Departamento de Ecología, Facultad de Ciencias, Universidad Católica de la Santísima Concepción, Concepción 4090541, Chile; carlos.lara@ucsc.cl
2 Centro de Investigación en Recursos Naturales y Sustentabilidad (CIRENYS), Universidad Bernardo O'Higgins, Santiago 8370993, Chile
3 Departamento de Física, Facultad de Ciencias, Universidad del Bío-Bío, Concepción 4051381, Chile
4 Centro FONDAP de Investigación en Dinámica de Ecosistemas Marinos de Altas Latitudes (IDEAL), Valdivia 5090000, Chile
5 UMMISCO, UMI 209, Sorbonne Université-IRD, 75006 Paris, France; cazelles@biologie.ens.fr
6 IBENS, UMR CNRS 8197, Eco-Evolution Mathématique, Ecole Normale Supérieure, 75005 Paris, France
7 Centro de Estudios Avanzados en Zonas Áridas, Coquimbo 1781681, Chile; marcelo.rivadeneira@ceaza.cl
8 Departamento de Biología Marina, Facultad de Ciencias del Mar, Universidad Católica del Norte, Coquimbo 1781421, Chile
9 Departamento de Biología, Universidad de La Serena, La Serena 1720256, Chile
10 Programa de Magister en Oceanografía, Universidad de Concepción, Concepción 4070386, Chile; richmunoz@udec.cl
11 Centro de Investigación de Estudios Avanzados del Maule (CIEAM), Vicerrectoría de Investigación y Postgrado & Departamento de Obras Civiles, Facultad de Ciencias de la Ingeniería, Universidad Católica del Maule, Talca 3460000, Chile; agalan@ucm.cl
12 Data Observatory Foundation, Santiago 7941169, Chile; alvaro.paredes@dataobservatory.net
13 Instituto de Ciencias Marinas y Limnológicas, Facultad de Ciencias, Universidad Austral de Chile, Valdivia 5090000, Chile; pablo.fierro@uach.cl
14 Departamento de Ciencias, Facultad de Artes Liberales and Bioengineering Innovation Center, Facultad de Ingeniería y Ciencias, Universidad Adolfo Ibáñez, Viña del Mar 2562340, Chile; bernardo.broitman@uai.cl
* Correspondence: gsaldias@ubiobio.cl

Abstract: Using 19 years of remotely sensed Enhanced Vegetation Index (EVI), we examined the effects of climatic variability on terrestrial vegetation of six protected areas along southwestern South America, from the semiarid edge of the Atacama desert to southern Patagonia (30°S–51°S). The relationship between satellite phenology and climate indices, namely MEI (Multivariate ENSO Index), PDO (Pacific Decadal Oscillation) and SAM (Southern Annular Mode) were established using statistical analyses for non-stationary patterns. The annual mode of phenological activity fluctuated in strength through time from the semiarid region to the border of southern Patagonia. Concomitantly, enhanced synchrony between EVI and climatic oscillations appeared over interannual cycles. Cross correlations revealed that variability in MEI was the lead predictor of EVI fluctuations over scales shorter than 4 months at lower latitudes and for the most poleward study site. The PDO was correlated with EVI over lags longer than 4 months at low latitude sites, while the SAM showed relationships with EVI only for sites located around 40°S. Our results indicate that the long-term phenological variability of the vegetation within protected areas along southwestern South America is controlled by processes linked to climate indices and that their influence varies latitudinally. Further studies over longer time scales will be needed to improve our understanding the impacts of climate change on vegetation condition and its effect over phenological variability.

Keywords: climatic change; vegetation index; MODIS; phenology; long-term variability

1. Introduction

Climatic variability has been identified as the lead driver of observed changes in phenological cycles worldwide [1–3]. Phenological changes have consequences that cascade

across the entire ecosystems: from altering the timing of flower emergence, and their mismatch with pollinators life cycles, to an earlier onset of greening and delayed senescence of forest canopies [4–7]. Climate-driven drought disturbs the phenology of forests in boreal, temperate, and tropical ecosystems, impacting tree growth and mortality [8,9]. On the other hand, the strong warming-induced trend for earlier spring and later autumn has changed the photosynthesis-mediated carbon uptake in the temperate forests of eastern North America during the past two decades [10]. Although changes in phenological patterns have been reported mostly for the northern hemisphere [11,12], the impacts of climate variability on the dynamics of vegetation phenology have a global reach and are expected to display a complex structure over space and time [13].

Understanding the association between climatic change and vegetation phenology requires long–term evaluation of the spatiotemporal interplay between oceanic conditions and land vegetation characteristics. Capturing vegetation characteristics solely based on in situ measures is challenging due to the large spatial heterogeneity across the scales [14]. To circumvent this shortcoming, spectral indices derived from remotely sensed platforms have been employed as a proxy to monitor annual and interannual variability from the field [15] to regional [16] and global scale [17]. With the proliferation of satellites and radiometric measurements, several vegetation indices have been developed among which the Enhanced Vegetation Index (EVI) and the Normalized Difference Vegetation Index (NDVI) have been more highlighted for their enhanced performance in capturing plant phenology [18,19].

In hydro-climatological studies, oceanic conditions and oscillations have been presented in the form of large-scale climate indices that capture patterns of heat and mass distribution in the atmosphere and oceans [20,21]. Among climate indices, ENSO (El Niño-Southern Oscillation) has been recognized as one of the leading modes of global climate variability, and other climatic modes, such as the Pacific Decadal Oscillation (PDO) or the Atlantic Multidecadal Oscillation (AMO) interact with ENSO to modulate phenological patterns of vegetation at a global scale [22,23].

The temporal dynamics of climate indices characterize the state of the coupled ocean—atmosphere systems across the entire Pacific ocean, which is tightly coupled to global-scale patterns of climatic variability, from interannual to decadal scales [24].

Using the spectral indices researchers have studied climate indices and vegetation phenology. For example the authors of Zhao et al. [25] have shown ENSO (El Niño-Southern Oscillation) as a key driver of interannual variability of vegetation phenology using NDVI. Besides climatic effects, the influence of precipitation and temperature on phenological activity has been studied in different regions (e.g., arid, semiarid, tropical) [26,27]. In the semi-arid climate of the middle east, the agricultural crops are severely stressed by heat and limited rainfall [28] while in Mediterranean areas, vegetation phenology is stressed during summer due to soil moisture depletion [29] and in southern Africa and South America the growth of vegetation is limited by water availability [30]. In temperate forest, the increase in air temperature has also altered vegetation phenological patterns (e.g., phenological advances of approximately 3–8 days for each °C increase of 1), vegetation activity and regional carbon cycling [10,31].

The impact of climate change is particularly important and more pronounced over biodiversity-rich areas [32]. The coast of Chile, extending along western south America from the Atacama desert to Patagonia region, spans 12 vegetation formations and 127 vegetation types [33]. This broad latitudinal gradient provides a model system to evaluate the impacts of climate variability on the spatio-temporal dynamics of vegetation phenology. Ecological studies have recognized the importance of climatic variability as a driver of changes in the productivity and composition of the different vegetation types found along this latitudinal gradient [34,35]. For example, long-term monitoring in semiarid central Chile has shown that vegetation dynamics are tightly linked to interannual changes in the ENSO-controlled precipitation regime [36].

Moreover, an ENSO-driven drought now extending for over a decade (2010–2020) in central Chile has imposed different trends on terrestrial productivity depending on latitude [37]. Similarly, the coupling of positive ENSO and SAM anomalies seem to underpin a pattern of increased forest fires across central and southern Chile over the same period during the last decade [21,38–40]. Together, these studies suggest that long-term climatic variability is impacting seems to modulate vegetation dynamics along western south America and that their effects are not homogeneous in space neither in space nor in time. However, the temporal climatic dynamics driving observed changes in vegetation dynamics have not been investigated to date.

Satellite-derived vegetation indices have been used before to assess the temporal variability of different vegetation ecosystems of Chile [29,30]. However, their ability to capture phenological heterogeneity and their linkages with large-scale climatic oscillations are currently lacking.

In this study, we evaluated the sensitivity of EVI to climatic variability along an extensive region characterized by heterogeneous biomass distribution and hypothesized that climatic oscillations have an asymmetric influence on the spatiotemporal phenological variability across the study region. To this end, the aim of this study was to comprehensively examine the effects of climatic variability on the EVI over multiple temporal scales, with an emphasis on the impacts that the time-varying climate has on the phenological patterns along the meridional extent. Section 2 introduces the study area and satellite data. Section 3 describes the main results evaluating the terrestrial plant phenology response to climatic oscillations along the latitudinal gradient. The discussion is presented in Section 4, emphasizing the differences in phenological responses to climate change. Finally, the main conclusions are highlighted in Section 5.

2. Data and Methodological Analysis

2.1. Study Area

The central–southern coast of Chile along the western Pacific coast of South America is characterized by a narrow semiarid region, where the Atacama desert, the driest on the planet, changes into a Mediterranean climate (30°S–37°S). While humidity in the semiarid region is provided mostly by seasonal coastal fog, the Mediterranean region is characterized by seasonal precipitation (>200 mm) concentrated during the austral winter months (June, July, August), which is subject to considerable interannual variability. On the other hand, the southern–austral region experiences a temperate climate (38°S–53°S), with year-round rainfall that can exceed 2000 mm, particularly south of 40°S [41–43].

The vegetation of the lower-latitude part of the coastal temperate sector, between 38 and 43°S, corresponds to Valdivian rainforest, dominated by species with wide leaves adapted to high humidity [44]. The Sub-Antarctic forest poleward of 47°S is dominated by deciduous Nothofagus species such as *Nothofagus pumilio* and *Nothofagus antarctica*, among others [44,45]. Due to the high endemism and its isolation, the Valdivian and Sub-Antarctic forests integrate a global biodiversity hotspot [46,47], which has been affected by human disturbances (selective logging and livestock grazing) and natural processes [48].

We focused our study on forested areas located within the boundaries of National Parks to tease out the potential effects of long-term human activities on vegetation (i.e., changes in land use and/or irrigation) from climate-driven phenological dynamics. In Chile, the conservation strategy that defines the legal boundaries and management plans for these protected areas follows that stated by the International Union for Conservation of Nature (IUCN) as: "a clearly defined geographical space, recognized, dedicated and managed, through legal or other effective means, to achieve the long-term conservation of nature with associated ecosystem services and cultural values". These areas generally include heterogeneous vegetation and land surface cover, for example rocky or glaciated areas, and are managed under the National System of Protected Wild Areas (SNASPE), which is administrated by the Chilean National Forestry Corporation (CONAF) [33,49]. We selected six national parks that spanned the vegetation gradient from the semi-arid edge of the

Mediterranean sector to the Cold Patagonian tundra, using cartography provided by the SNASPE to define the units of study (Figure 1). The selected parks were: Fray Jorge (30°S), La Campana (32°S), Alerce Costero (40°S), Tantauco (43°S), Laguna San Rafael (47°S), and Torres del Paine (51°S) (Table 1).

Table 1. Vegetation formations in National Parks of this study according to Pliscoff and Fuentes-Castillo [33].

| National Park	Area (km^2)	Year Created	Vegetation Formation
(1) Fray Jorge (30°S)	86.06	1941	Desertic scrub
(2) La Campana (32°S)	78.18	1967	Deciduous forest Sclerophyllous forest Alpine dwarf scrub
(3) Alerce Costero (40°S)	236.14	2010	Valdivian Laured-Leaved Forest Fitzroya Forest
(4) Tantauco (43°S)	1016.4	2005	Deciduous forest
(5) San Rafael (47°S)	18,693.40	1959	Deciduous forest Sclerophyllous forest Evergreen forest Alpine dwarf scrub Deciduous shrub Evergreen shrub Peatbog
(6) Torres del Paine (51°S)	2216.47	1959	Deciduous forest Evergreen forest Alpine dwarf scrub Matorral arborescent Deciduous shrub
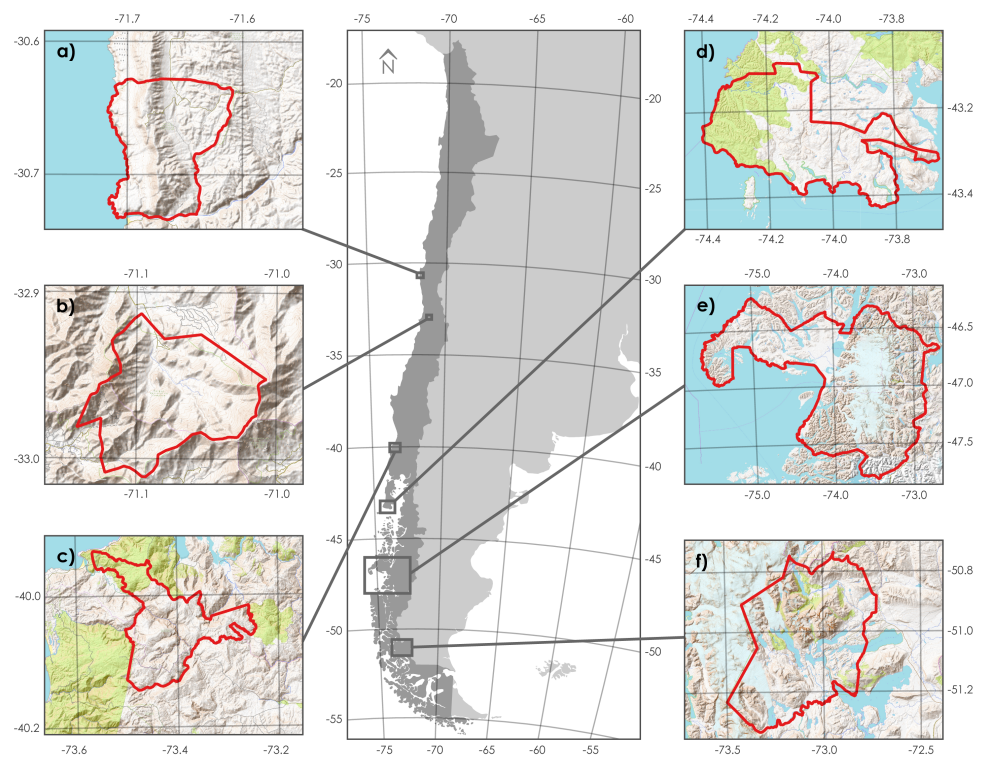
Figure 1. Map of the study area showing National Parks: (**a**) Fray Jorge, (**b**) La Campana, (**c**) Alerce Costero, (**d**) Tantauco, (**e**) San Rafael and, (**f**) Torres del Paine.

2.2. Phenology and Climatic Data

We used satellite images of the Enhanced Vegetation Index (EVI; MOD13Q1 product, version 6) from the Moderate Resolution Imaging Spectroradiometer (MODIS) sensor onboard the Terra satellite. EVI is an L3 product with a resolution of 250 m, generated every 16 days from daily images. The EVI algorithm choose the best available pixel value (i.e., low clouds, low view angle, and the highest NDVI/EVI value) from all the acquisitions from the 16 days period. We downloaded and analyzed a time series of images from February 2000 to December 2018. Using the polygon of each site, we generated an internal 250-m buffer for each park and the corresponding EVI time series (e.g., [50]). Our analysis aimed to capture biospheric responses to climate, and hence they included the totality of the park area and the different kinds of vegetation within (see Table 1). Zonal statistics per observation (scene) were calculated for each park, at each time. This results in a temporal series of one data point every 16 days, for each park (the mean). That data were aggregated by month using a weighted mean, in order to match the temporal resolution of the climatic data, with the weight consisting in the number of valid pixels per scene at each time and park. When there was only one scene per month, that observation is used. When there was two, the weighted mean is computed. All data extracting and processing were implemented in Python and the MODIS imagery re-projection and cropping were carried out using the Modis Reprojection Tool.

In order to identify the long-term relationships between climatic oscillations and phenological variability, we examined three climatic indices: MEI, PDO and SAM, which were obtained from the National Weather Service website (www.cpc.ncep.noaa.gov, accessed on 1 September 2020) of the National Oceanic and Atmospheric Administration (NOAA). These three monthly climatic indices strongly influence climate along western south America, and their variability modulates changes in precipitation and streamflow along the study region [51,52].

2.3. Data Analysis

We performed a wavelet analysis on MODIS phenological data to explore the interannual variability in phenological indices. Additionally, a bootstrapping method was used to evaluate the significance of wavelet spectra (more details are found in [53]). The relative importance of frequencies for each time step is represented in the time–frequency plane to form the local wavelet power spectrum (WPS). Here, we used the Morlet wavelet to detect the characteristics in phenology fluctuations, which according to Cazelles et al. [54] is defined as:

$$\psi(t) = \pi^{-1/4}exp(-i\omega_0 t)exp(-t^2/2) \tag{1}$$

where $exp(-i\omega_0 t)$ is the product of a complex sinusoidal, $\pi^{-1/4}$ is a normalization factor to ensure unit variance and ω_0 represent the central angular frequency of the wavelet [54]. One of the key advantages of a continuous wavelet function is the mathematical relationship between the wavelet scale and its frequency a and its frequency f. We also computed the global WPS where all wavelet coefficients of the same frequency f were averaged. The global WPS is defined by Cazelles et al. [54] as:

$$\overline{WPS}_x(f) = \frac{\sigma_x^2}{T} \int_0^T \|W_x(f,\tau)\|^2 d\tau \tag{2}$$

where σ_x^2 is the variance of time-series (EVI), T is the time duration of the time series (2000–2018) and $W_x(f,\tau)$ is the wavelet transform of the $x(t)$. All analyses were performed using the MATLAB wavelet scripts (www.biologie.ens.fr/~cazelles/bernard/Research.html, accessed on 6 April 2021). To quantify the co-variation between EVI and climate indices we computed the wavelet coherence, which measures the correlation between the spectra of two series [55] and is defined as:

$$R_{x,y}(f,\tau) = \frac{\| < W_{x,y}(f,\tau) > \|}{\| < W_{x,x}(f,\tau) > \|^{1/2} \| < W_{y,y}(f,\tau) > \|^{1/2}} \tag{3}$$

where $<>$ indicates a smoothing operator in time and scale, $W_{x,y}(f,\tau)$ is the wavelet co–spectrum of the two time series $x(t)$ and $y(t)$, respectively, $W_{x,x}(f,\tau)$ and $W_{y,y}(f,\tau)$ are the wavelet transform of the $x(t)$ and $y(t)$. The wavelet coherence ($R_{x,y}(f,\tau)$) is equal to 1 when there is a perfect linear relation between the frequency of two temporal signals, and is equal to 0 when signals $x(t)$ and $y(t)$ are independent with no common frequencies at a particular temporal scale [54,56]. Finally, we computed cross-correlations between the EVI signal and the climatic indices for each park with time lags from 0 to 7 months. The semi-annual lag was chosen as the maximum delay where the impact of climate-driven seasonal variability could be detected on the phenological cycle.

3. Results

Vegetation productivity, using EVI as proxy, showed a significant interannual variability in the intensity of the 1-year period—the phenological band. In general, WPS of EVI revealed a unique and significant annual signal, that persisted throughout the study period for all evaluated parks (Figure 2), except for La Campana and Torres del Paine, where this phenological signal was interrupted. Changes in EVI were significant just during 2001–2006, 2010–2013 and 2015–2017 for La Campana (Figure 2b) and during 2001–2009 and 2012–2018 for Torres del Paine, being the last period characterized by low WPS (Figure 2f). Another low-powered but significant oscillation of about 2 year was also detected during 2006–2009 and 2016–2017 at this sub-antarctic region (Figure 2f). This shifting in the phenological signal intensity across the latitudinal range suggests an external time-varying forcing of the annual cycle of productivity.
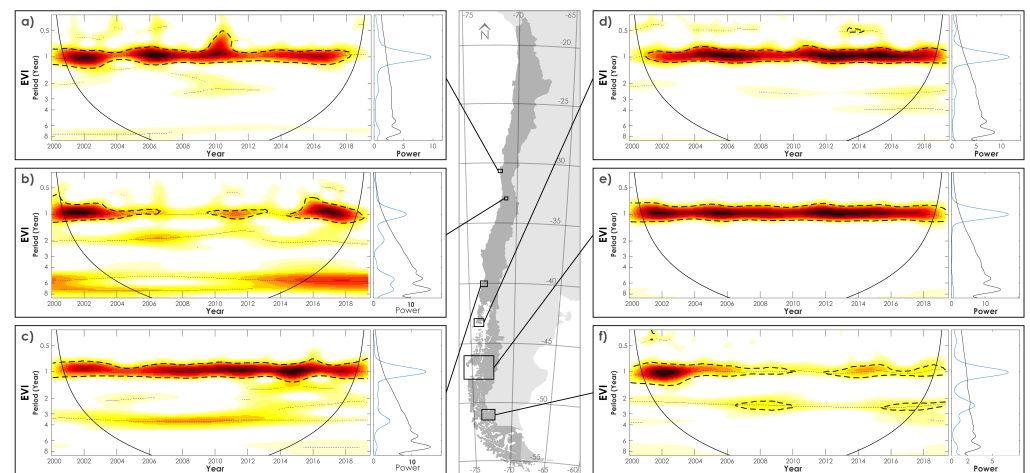
Figure 2. Wavelet analysis of EVI monthly data between 2000 and 2018 in (**a**) Fray Jorge, (**b**) La Campana, (**c**) Alerce Costero, (**d**) Tantauco, (**e**) San Rafael and (**f**) Torres del Paine. The left panels show local wavelet power spectrum. The color code for power values is from white (low power values) to dark red (high power values). The dot-black lines indicate the 95% significant areas obtained by adapted bootstrapping [57] and the cone of influence (bold-black lines) indicates the wavelet domain where computations are not influenced by edge effects (see [56]). The right panels show the global wavelet power spectrum for the period examined (2000–2018) with the black line showing a 95% confidence interval obtained by adaptive bootstrapping (note that they have different scale for better visualization).

Figure 3 shows the WPS for all climate indices studied. While the MEI showed a high-power significant oscillation just for the 2–3 year period between 2007 and 2016 (Figure 3a), the PDO denoted a transient and significant 1.5–2 year oscillation during 2001–2003 and 2007–2013, with another significant oscillation of 2–4 years for the 2013–2016 period (Figure 3b). Conversely, high-power spectra oscillation for SAM were less frequent relative to MEI and PDO, with significant WPS occurring around a 6–7 year band for the 2010–2016 period (Figure 3c).

Transient and significant synchrony between EVI and MEI was revealed over multi-year frequencies (1 to 4-year) for the different parks. A significant and persistent 2–3-year component was present between 2004 and 2011 (Fray Jorge, Tantauco and Torres del Paine), and 2003 and 2006 (La Campana and Alerce Costero), while a significant 4-year periodic component was observed between 2008 and 2016 (San Rafael), 2010 and 2015 (La Campana), and 2012 and 2015 (Alerce Costero) (Figure 4). The synchrony between EVI and PDO showed a more consistent pattern across time and space. From 2010 to 2016, a periodic 1-year oscillation was observed along the entire studied area, while a transient and broad synchronous band over a 2–3-year period was observed between 2001 and 2005 and 2008 and 2015 in Fray Jorge, 2001 and 2013 in Tantauco and 2002 and 2011 in Torres del Paine (Figure 5). The temporal coherence between EVI and SAM revealed a 2–4 year joint band in Fray Jorge (2008–2013), La Campana (2006–2015), Alerce Costero (2002–2009) and Torres del Paine (2002–2007), and a 4–6 year oscillation appeared significant in Tantauco (2009–2015) and San Rafael (2003–2007) (Figure 6). In several portions of the analysis, intra-anual (0.5-year) modes were significant, yet they should be interpreted with caution due to their short duration and the coarse temporal resolution of our data.
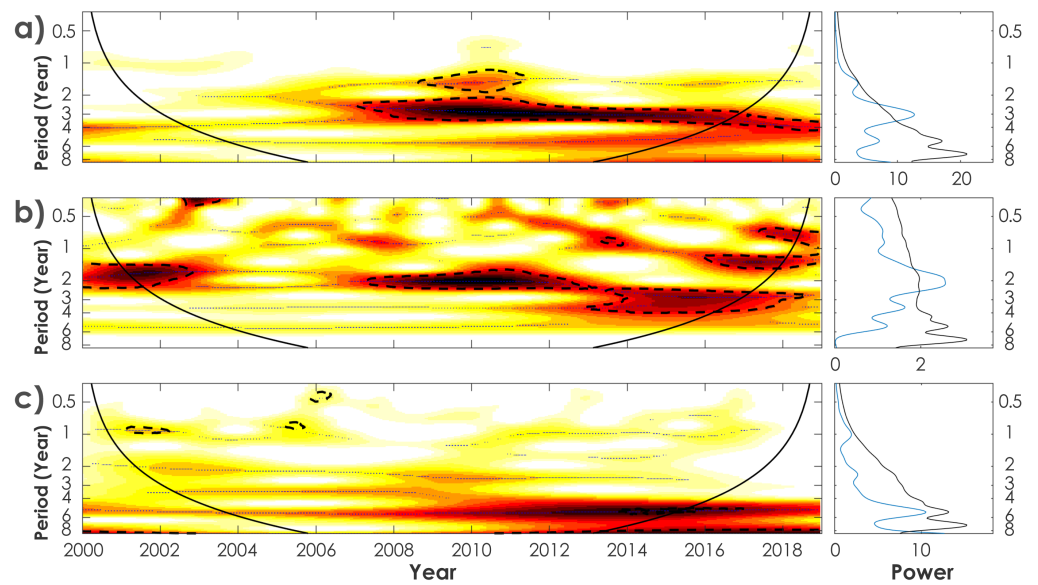
Figure 3. Wavelet analysis of climatic indices monthly data between 2000 and 2018. (**a**) MEI, (**b**) PDO and (**c**) SAM. The left panels show local wavelet power spectrum. The color code for power values is from white (low power values) to dark red (high power values). The dot-black lines indicate the 95% significant areas obtained by adapted bootstrapping [57] and the cone of influence (bold-black lines) indicates the wavelet domain where computations are not influenced by edge effects (see [56]). The right panels show the global wavelet power spectrum for the period examined (2000–2018) with the black line showing a 95% confidence interval obtained by adaptive bootstrapping (note that they have different scale for better visualization).
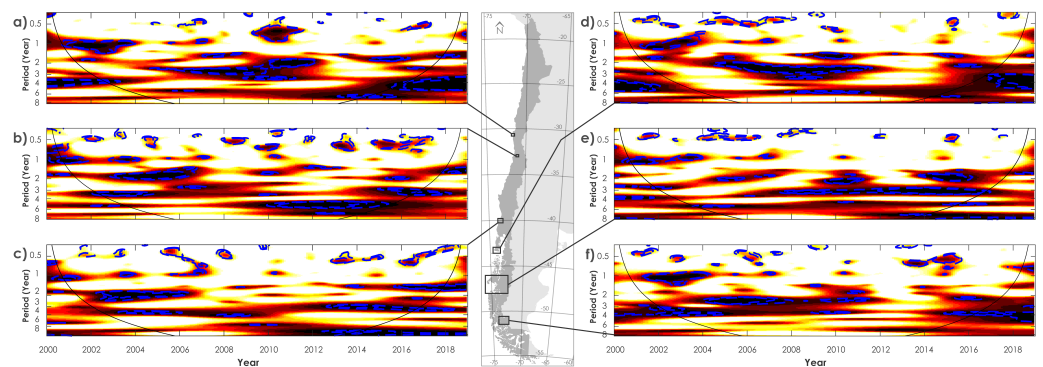

Figure 4. Wavelet coherence between the EVI and MEI temporal signal in national parks. (**a**) Fray Jorge, (**b**) La Campana, (**c**) Alerce Costero, (**d**) Tantauco, (**e**) San Rafael and (**f**) Torres del Paine. The colors are coded from yellow (low coherence) to dark red (high coherence). The dotted-dashed blue lines show the 95% and the 90% significance levels computed based on bootstrapped series. The cone of influence (black line) indicates the region not influenced by edge effects (see [56]).

Figure 5. Wavelet coherence between the EVI and PDO temporal signal in national parks. (**a**) Fray Jorge, (**b**) La Campana, (**c**) Alerce Costero, (**d**) Tantauco, (**e**) San Rafael and (**f**) Torres del Paine. The colors are coded from yellow (low coherence) to dark red (high coherence). The dotted-dashed blue lines show the 95% and the 90% significance levels computed based on bootstrapped series. The cone of influence (black line) indicates the region not influenced by edge effects (see [56]).
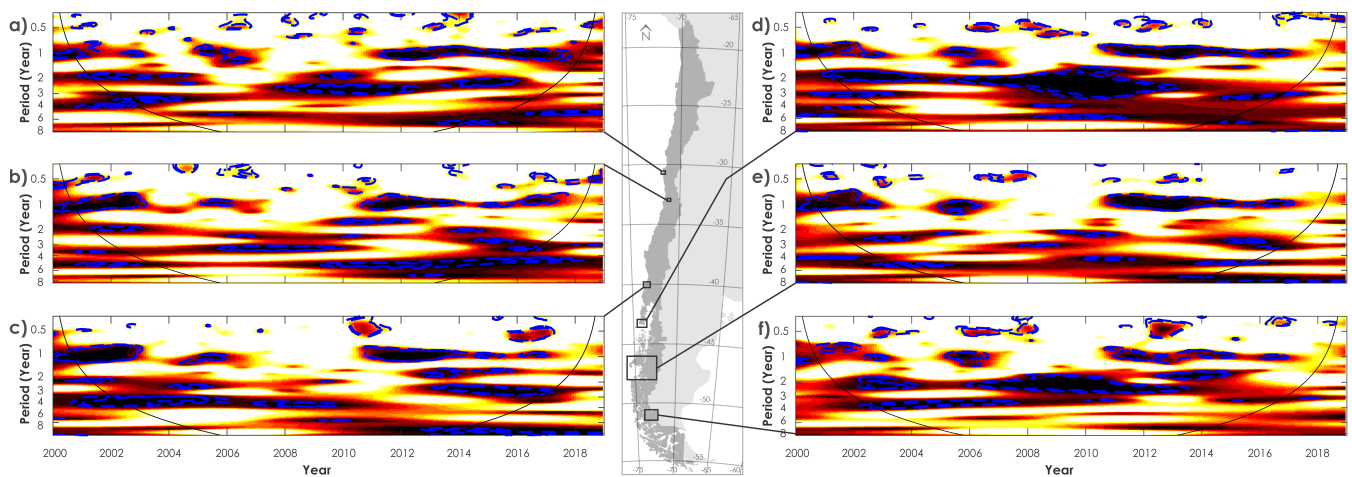

Figure 6. Wavelet coherence between the EVI and SAM temporal signal in national parks. (**a**) Fray Jorge, (**b**) La Campana, (**c**) Alerce Costero, (**d**) Tantauco, (**e**) San Rafael and (**f**) Torres del Paine. The colors are coded from yellow (low coherence) to dark red (high coherence). The dotted-dashed blue lines show the 95% and the 90% significance levels computed based on bootstrapped series. The cone of influence (black line) indicates the region not influenced by edge effects (see [56]).
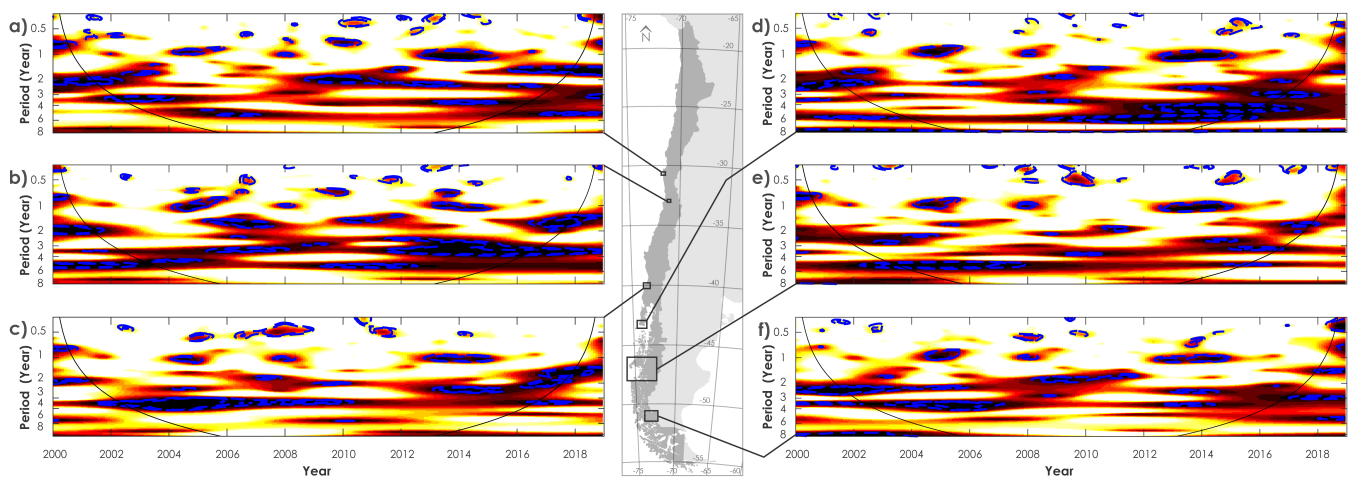
Lagged correlations between climatic indices and EVI are presented in Figure 7. Climate indices lead the analysis and positive correlations mean that the corresponding climate index and EVI are in phase (e.g., positive MEI before leads to positive EVI after). At Fray Jorge Park, EVI showed a quick and weakly significant positive relationship with MEI that persisted for 3 months. For PDO, the response was negative at lag-0 and switched to a positive relationship over lags between 6 and 7 months. No significant cross-correlations were observed with the SAM at this site (Figure 7a). A similar pattern was observed in La Campana National Park, but the positive cross-correlation between EVI and MEI persisted for 5 months and the positive significant lags with PDO appeared at 6 and 7 months (Figure 7b). Alerce Costero and Tantauco National Parks, located ca. 10 degrees south of La Campana, did not share the lagged correlation structure with the Mediterranean region. No significant correlations with MEI were observed, but there were significant negative associations with PDO between 2- and 5-month lags for Alerce Costero and 4-month lag for Tantauco, which also showed a significant and positive zero-

lag correlation with SAM (Figure 7c,d, respectively). In the case of San Rafael National Park, significant and positive correlations were observed at lag-0 for both PDO and SAM, and also for SAM at 1 month (Figure 7e), while for Torres del Paine, the most austral National Park, EVI showed significant positive correlations with MEI at 3–4 months and negative at 0 and 4–5 months with PDO (Figure 7f).
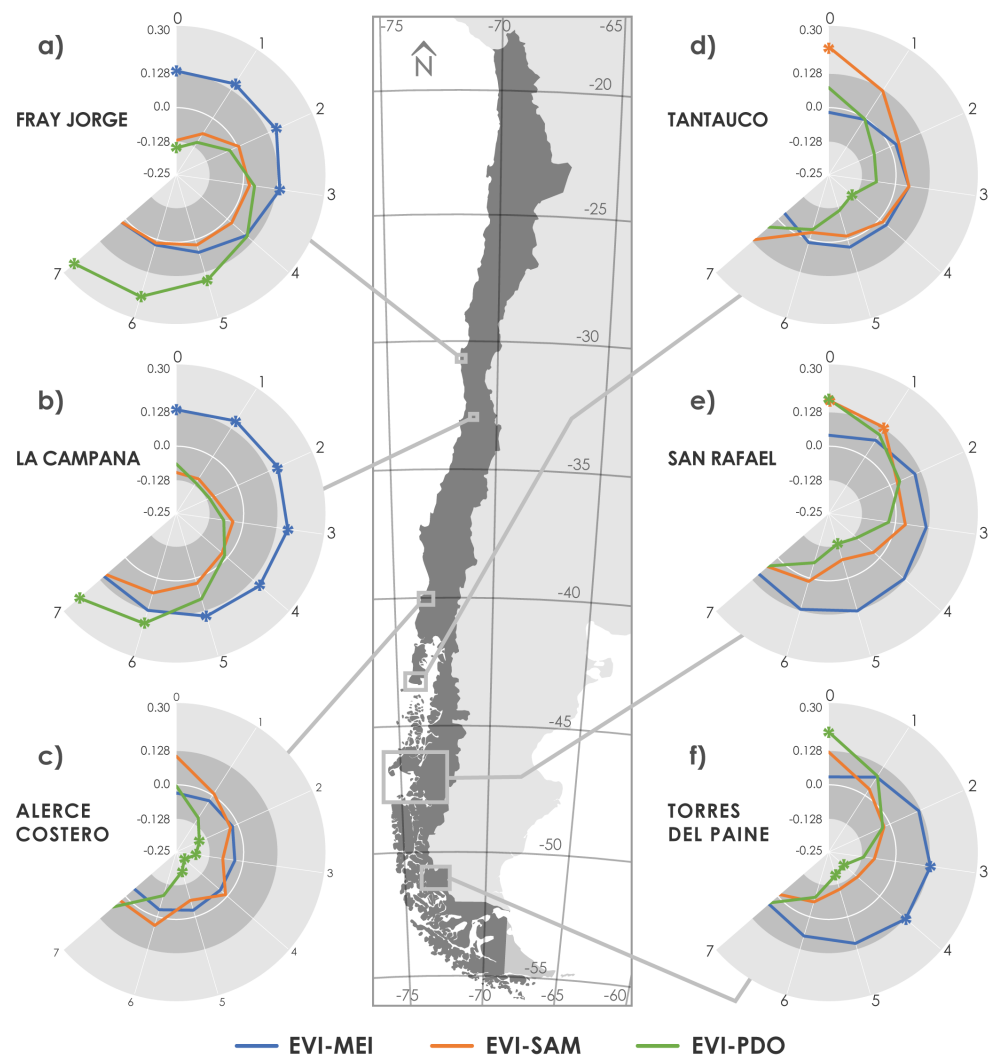

Figure 7. Lagged correlations between EVI and MEI (blue line), EVI and SAM (orange line) and EVI and PDO (green line) in each park (see order in Figure 1). The external numbers around the ring show the respective lag (0 to 7) between the climatic data and EVI. Points marked with asterisk and on the light gray zone of the circle are statistically significant at 5%.

4. Discussion

Our work shows a persistent and time-varying association between phenological patterns and different climatic oscillations over a broad range of vegetational formations spread along the western coast of south America. These results provide new insights on how the spatio-temporal variable natural climate forcing modulates the physiological status in terrestrial ecosystems over global, regional and local scales (see references in [58,59]) and influences the provision of essential environmental variables.

Due to the critical role that vegetation plays in the global biogeochemical and hydrological cycles, and the services we derive from them, it is relevant to understand how plant dynamics respond to global climatic oscillations over multiples scales [60]. Our study highlights the impacts that tropical ocean–atmosphere dynamics have on seasonal vegetation

activity, ranging from the semi-arid Mediterranean scrub down to the sub Antarctic tundra of Patagonia. Previous studies evidence the strong impact of ENSO events (e.g., extreme MEI anomalies) on vegetation of the Southern Hemisphere [34,51]. The warm phase of ENSO (El Niño) covaries with severe drought events in some regions (e.g., Australia, southeast Asia, northeastern South America), whereas the cold phase (La Niña) is associated with droughts in western south America [22,61]. In concomitance with ENSO, PDO also appears as a driver of the phenological patterns along western south America, mediated by the meridional displacement of the subtropical gyre, changes in the pattern of the winds, and SST anomalies [43,62,63].

Changes in the precipitation pattern associated with negative phases of PDO are related to a drying trend in central Chile (30°S–40°S) over the last 30 years [42,43,64]. The detrimental effects of the reduced rainfall are evidenced as changes in the vegetation growing-season during the so-called megadrought period (2010–2018) in central Chile [37,64]. The uninterrupted sequence of dry years, i.e., years with a rainfall deficit, coincided with a negative EVI signal over pasture lands and areas with native forests cover. When coupled with climate effects (e.g., warming), these intense drought periods could promote fire activity (frequency and severity), mainly in areas with extensive plantations of non-native forests, native sclerophyll forests, and scrublands, vegetation types that largely determine the primary productivity patterns in central Chile [37,65]. While in northern Patagonia, both coastal ocean and land biological processes are forced by climatic variability over multiple temporal scales [66].

In the Southern Hemisphere, where instrumental records are sparse and relatively short, the opportunities for understanding the large-scale dynamical mechanisms driving climate variability are limited [67]. According to Marshall [68], the SAM oscillation is defined by the gradient between the high-pressure belt at medium latitudes and the lower pressures around coastal Antarctica. As such, it is calculated as the zonally averaged pressure difference between 40°S and 65°S. SAM oscillations are phase-dependent with ENSO, e.g., when a positive phase of ENSO (El Niño) coincide with a negative phase of SAM (Figure A2), climate anomalies dominate south of 40°S [69], generating extreme conditions due to high solar irradiation and reduced precipitation [66,70]. Such phase-locking could drive part of the observed changes in phenological activity, e.g., weak amplitude (see Figure 7).

Despite the low but significant lagged-effect of ENSO and PDO on the phenological pattern for the 43°S–52°S zone, our results strengthen the conclusion that the teleconnection between ocean—atmosphere oscillations are evident in the coast of South America. Multiple studies have associated ENSO with spring rainfall in southern China [71] and across western North America [72]. Although these climatic drivers have not been formally established, following a lack of in situ data, our results can be used to assess the impacts of climatic teleconnection processes with local phenology patterns.

EVI provides a consistent measure of greenness and improves sensitivity over dense vegetation conditions closely related to the seasonal variation of biological activity and their sensitivity to climatic oscillations over multiple time-lag relationships [73]. Throughout the study period (2000–2018), we observed significant time-lagged effects of the local vegetation to global climatic oscillations. However, in Fray Jorge National Park, several long-term studies that investigated the effects of climatic forces on population dynamics of wild rodents suggest that pulses of higher rainfall, induced by ENSO, impact ecological processes over multiple scales of organizations (e.g., [74–76]), including human communities and land use. Garreaud et al. [37] showed the effects of climate variability on rainfall along a latitudinal gradient spanning most of Chile and including all types of vegetation. It showed that, along the central region (30–38°S), a large negative rainfall anomaly (nicknamed Megadrought) had a major impact on the gross plant productivity (as measured by the EVI index) during the 2010–2015 period, disproportionally impacted the semi-arid shrublands of north–central Chile (30–33°S) and the coastal region south of 30°S, following the curtailed rainfall during this period. In contrast, positive but patchy anomalies in

EVI were recorded between 34°S and 37°S, which were associated to forest plantations involving non-native species with a rapid initial growth in leaf area [77]. Thus, the complex interplay among climate-driven variability in air temperature, rainfall, and other variables in the latitudinal gradient of Chile, in addition to the different vegetation types (Table 1), should result in marked differences in phenological activity (evidenced in the power spectra for different parks; Figures 2 and A1) in our study. Therefore, it is essential to couple the impact of climate variability with the patterns of air temperature, precipitations, and hydrological regimes to further inspect the contrasting impacts of climate events on the plant productivity and phenology along western South America.

Remote sensing vegetation indices can be used as a robust tool to assist decision-making for the conservation and management of areas with high vegetation endemism. Time-lagged responses provide us with insights into how earlier conditions impact vegetation activity. In most open shrubs, at middle and low latitudes, climatic forcing reveals their significant effect on vegetation growth [73]. This study highlights the complexity in biogeographic climate–vegetation biomass effects that should be considered in predictive climate models of phenological variations along western South-America.

5. Summary

The Pacific coast of western South America has a wide latitudinal range of climate variability, with consequent change in vegetation communities. In recent years there has been increasing interest regarding the effects of climatic oscillations on phenological patterns. Our study demonstrated that the response of EVI to capture the annual cycle of vegetative communities in the temperate climate region minimizes canopy—soil variations and improves sensitivity over dense vegetation conditions. On the other hand, the MEI and SAM indices showed an effect on multiple lags along the latitudinal gradient. Coincidentally, PDO also presents an effect (4–6 month lags) along the study area. Future studies should carefully analyze the PDO as the ENSO/SAM variability only partially determines the phenological patterns along our broad study region. To this end, our results provide a first step towards the design of conservation strategies that integrate climatic information into the managing and monitoring of essential environmental variables, chiefly the phenology terrestrial productivity, along the Pacific coast of western South America.

Author Contributions: C.L., B.C., M.M.R., Á.L.P. and B.R.B. conceived the research; C.L., B.C., M.M.R., G.S.S., A.L.P. working in data curation and formal analysis; C.L., B.C., M.M.R., G.S.S., R.M., A.G., Á.L.P., P.F. and B.R.B. writing the original draft and editing the final version. All authors have read and agreed to the published version of the manuscript.

Institutional Review Board Statement: Not applicable.

Informed Consent Statement: Not applicable.

Data Availability Statement: The vegetation indices from the MODIS-TERRA data product were retrieved from the online Data Pool, courtesy of the NASA Land Processes Distributed Active Archive Center (LP DAAC), USGS/EarthResources Observation and Science (EROS) Center, Sioux Falls, South Dakota (https://lpdaac.usgs.gov/products/mod13q1v006/, accessed on 6 April 2021). Climatic indices are available in National Weather Service website (www.cpc.ncep.noaa.gov, accessed on 6 April 2021) of the National Oceanic and Atmospheric Administration (NOAA).

Conflicts of Interest: The authors declare no conflict of interest. The funders had no role in the design of the study; in the collection, analyses, or interpretation of data; in the writing of the manuscript, or in the decision to publish the results.

Appendix A

In this contribution, we also showed the NDVI (Normalized Difference Vegetation Index)'s temporal trends (Figure A1). As EVI, the NDVI also serves for detecting temporal changes in vegetation phenological activity. EVI have a greater dynamic range than NDVI to capture the phenological cycle, due to the fact that NDVI is mainly saturated in the red band region of the electromagnetic region where the energy is strongly absorbed by pigments [78,79] and also these values strongly tend to decrease in the presence of high background amounts of dry biomass. Moreover, NDVI varies depending the chlorophyll—the concentration and amount of vegetation biomass saturating when both chlorophyll and biomass present high levels [78,80]. For example, in the Chiloé Island Ecosystem, recognized as a biodiversity "hotspot", NDVI is susceptible to uncertainty of capturing the annual photosynthetic cycle [79]. EVI perform well under high aerosol loads (which may add significant noise to the signal), biomass burning conditions and topographic effect [78]. However, the temporal co-evolution of EVI and NDVI showed in general complementary patterns across the study region. In terms of the effects of climatic variability over both EVI and NDVI, our results showed the asymmetrical response of the phenological signal.
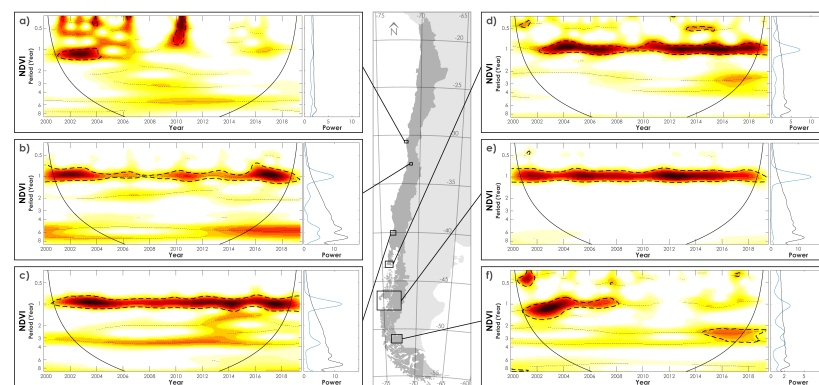

Figure A1. Wavelet analysis of NDVI monthly data between 2000 and 2018 in (**a**) Fray Jorge, (**b**) La Campana, (**c**) Alerce Costero, (**d**) Tantauco, (**e**) San Rafael and (**f**) Torres del Paine. The left panels show the local wavelet power spectrum. The color code for power values is from white (low power values) to dark red (high power values). The dot-black lines indicate the 95% significant areas obtained by adapted bootstrapping [57] and the cone of influence (bold-black lines) indicates the wavelet domain where computations are not influenced by edge effects (see [56]). The right panels show the global wavelet power spectrum for the period examined (2000–2018), with the black line showing a 95% confidence interval obtained by adaptive bootstrapping.
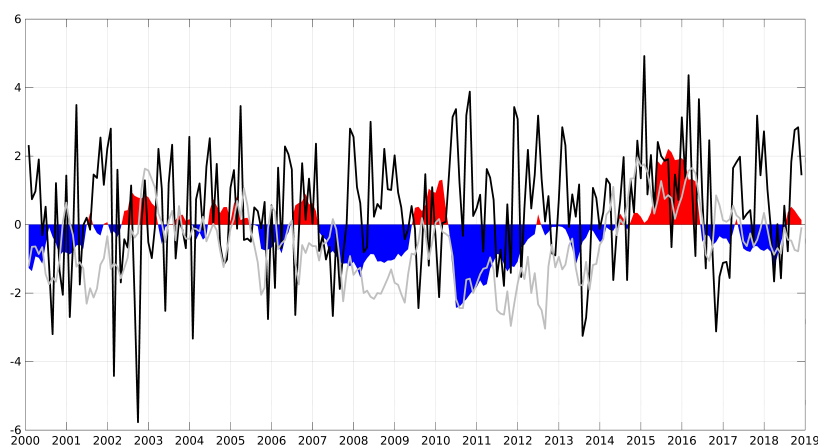
Figure A2. Time series of Climate indices: Multivariate ENSO Index (MEI; red/blue), Southern Annular Mode (SAM; black line), and Pacific Decadal Oscillation (PDO; grey line).

References

1. White, M.A.; Hoffman, F.; Hargrove, W.W.; Nemani, R.R. A global framework for monitoring phenological responses to climate change. *Geophys. Res. Lett.* **2005**, *32*. [CrossRef]
2. Donnelly, A.; Caffarra, A.; O'Neill, B.F. A review of climate-driven mismatches between interdependent phenophases in terrestrial and aquatic ecosystems. *Int. J. Biometeorol.* **2011**, *55*, 805–817. [CrossRef] [PubMed]
3. Renner, S.S.; Zohner, C.M. Climate change and phenological mismatch in trophic interactions among plants, insects, and vertebrates. *Annu. Rev. Ecol. Syst.* **2018**, *49*, 165–182. [CrossRef]
4. Cleland, E.E.; Chuine, I.; Menzel, A.; Mooney, H.A.; Schwartz, M.D. Shifting plant phenology in response to global change. *Trends Ecol. Evol.* **2007**, *22*, 357–365. [CrossRef] [PubMed]
5. Inouye, D.W. Effects of climate change on phenology, frost damage, and floral abundance of montane wildflowers. *Ecology* **2008**, *89*, 353–362. [CrossRef]
6. Seidl, R.; Thom, D.; Kautz, M.; Martin-Benito, D.; Peltoniemi, M.; Vacchiano, G.; Wild, J.; Ascoli, D.; Petr, M.; Honkaniemi, J.; et al. Forest disturbances under climate change. *Nat. Clim. Chang.* **2017**, *7*, 395–402. [CrossRef]
7. Beard, K.H.; Kelsey, K.C.; Leffler, A.J.; Welker, J.M. The missing angle: Ecosystem consequences of phenological mismatch. *Trends Ecol. Evol.* **2019**, *34*, 885–888. [CrossRef] [PubMed]
8. Allen, C.D.; Macalady, A.K.; Chenchouni, H.; Bachelet, D.; McDowell, N.; Vennetier, M.; Kitzberger, T.; Rigling, A.; Breshears, D.D.; Hogg, E.T.; et al. A global overview of drought and heat-induced tree mortality reveals emerging climate change risks for forests. *For. Ecol. Manag.* **2010**, *259*, 660–684. [CrossRef]
9. Klos, R.J.; Wang, G.G.; Bauerle, W.L.; Rieck, J.R. Drought impact on forest growth and mortality in the southeast USA: An analysis using Forest Health and Monitoring data. *Ecol. Appl.* **2009**, *19*, 699–708. [CrossRef]
10. Keenan, T.F.; Gray, J.; Friedl, M.A.; Toomey, M.; Bohrer, G.; Hollinger, D.Y.; Munger, J.W.; O'Keefe, J.; Schmid, H.P.; Wing, I.S.; et al. Net carbon uptake has increased through warming-induced changes in temperate forest phenology. *Nat. Clim. Chang.* **2014**, *4*, 598–604. [CrossRef]
11. Piao, S.; Fang, J.; Zhou, L.; Ciais, P.; Zhu, B. Variations in satellite-derived phenology in China's temperate vegetation. *Glob. Chang. Biol.* **2006**, *12*, 672–685. [CrossRef]
12. Ma, Q.; Huang, J.G.; Hänninen, H.; Berninger, F. Reduced geographical variability in spring phenology of temperate trees with recent warming. *Agric. For. Meteorol.* **2018**, *256–257*, 526–533. [CrossRef]
13. Yuan, H.; Wu, C.; Gu, C.; Wang, X. Evidence for satellite observed changes in the relative influence of climate indicators on autumn phenology over the Northern Hemisphere. *Glob. Planet Chang.* **2020**, *187*, 103131. [CrossRef]
14. Maignan, F.; Bréon, F.M.; Bacour, C.; Demarty, J.; Poirson, A. Interannual vegetation phenology estimates from global AVHRR measurements: Comparison with in situ data and applications. *Remote Sens. Environ.* **2008**, *112*, 496–505. [CrossRef]
15. Jamshidi, S.; Zand-Parsa, S.; Niyogi, D. Assessing Crop Water Stress Index of Citrus Using In-Situ Measurements, Landsat, and Sentinel-2 Data. *Int. J. Remote Sens.* **2021**, *42*, 1893–1916. [CrossRef]
16. Wang, X.; Zhang, S.; Feng, L.; Zhang, J.; Deng, F. Mapping Maize Cultivated Area Combining MODIS EVI Time Series and the Spatial Variations of Phenology over Huanghuaihai Plain. *Appl. Sci.* **2020**, *10*, 2667. [CrossRef]
17. Ye, W.; van Dijk, A.I.; Huete, A.; Yebra, M. Global trends in vegetation seasonality in the GIMMS NDVI3g and their robustness. *Int. J. Appl. Earth Obs. Geoinf.* **2021**, *94*, 102238. [CrossRef]
18. Kowalski, K.; Senf, C.; Hostert, P.; Pflugmacher, D. Characterizing spring phenology of temperate broadleaf forests using Landsat and Sentinel-2 time series. *Int. J. Appl. Earth Obs. Geoinf.* **2020**, *92*, 102172. [CrossRef]

19. Sarvia, F.; De Petris, S.; Borgogno-Mondino, E. Exploring Climate Change Effects on Vegetation Phenology by MOD13Q1 Data: The Piemonte Region Case Study in the Period 2001–2019. *Agronomy* **2021**, *11*, 555. [CrossRef]

20. Gore, M.; Abiodun, B.J.; Kucharski, F. Understanding the influence of ENSO patterns on drought over southern Africa using SPEEDY. *Clim. Dyn.* **2020**, *54*, 307–327. [CrossRef]

21. Sarricolea, P.; Serrano-Notivoli, R.; Fuentealba, M.; Hernández-Mora, M.; de la Barrera, F.; Smith, P.; Meseguer-Ruiz, Ó. Recent wildfires in Central Chile: Detecting links between burned areas and population exposure in the wildland urban interface. *Sci. Total Environ.* **2020**, *706*, 135894. [CrossRef]

22. Woodward, F.; Lomas, M.; Quaife, T. Global responses of terrestrial productivity to contemporary climatic oscillations. *Philos. Trans. R. Soc. B Biol. Sci.* **2008**, *363*, 2779–2785. [CrossRef]

23. Ito, A. Decadal variability in the terrestrial carbon budget caused by the Pacific Decadal Oscillation and Atlantic Multidecadal Oscillation. *J. Meteorol. Soc. Ser. II* **2011**, *89*, 441–454. [CrossRef]

24. Dätwyler, C.; Grosjean, M.; Steiger, N.J.; Neukom, R. Teleconnections and relationship between the El Niño–Southern Oscillation (ENSO) and the Southern Annular Mode (SAM) in reconstructions and models over the past millennium. *Clim. Past* **2020**, *16*, 743–756. [CrossRef]

25. Zhao, L.; Dai, A.; Dong, B. Changes in global vegetation activity and its driving factors during 1982–2013. *Agric. For. Meteorol.* **2018**, *249*, 198–209. [CrossRef]

26. Ficetola, G.F.; Maiorano, L. Contrasting effects of temperature and precipitation change on amphibian phenology, abundance and performance. *Oecologia* **2016**, *181*, 683–693. [CrossRef] [PubMed]

27. Liu, Q.; Fu, Y.H.; Zeng, Z.; Huang, M.; Li, X.; Piao, S. Temperature, precipitation, and insolation effects on autumn vegetation phenology in temperate China. *Glob. Chang. Biol.* **2016**, *22*, 644–655. [CrossRef] [PubMed]

28. Jamshidi, S.; Zand-Parsa, S.; Niyogi, D. Physiological responses of orange trees subject to regulated deficit irrigation and partial root drying. *Irrig. Sci.* **2021**, *39*, 441–455. [CrossRef]

29. Gordo, O.; Sanz, J.J. Impact of climate change on plant phenology in Mediterranean ecosystems. *Glob. Chang. Biol.* **2010**, *16*, 1082–1106. [CrossRef]

30. Zhang, X.; Hodges, J.C.; Schaaf, C.B.; Friedl, M.A.; Strahler, A.H.; Gao, F. Global vegetation phenology from AVHRR and MODIS data. In Proceedings of the IGARSS 2001, Scanning the Present and Resolving the Future, IEEE 2001 International Geoscience and Remote Sensing Symposium (Cat. No. 01CH37217), Sydney, Australia, 9–13 July 2001; Volume 5, pp. 2262–2264.

31. Richardson, A.D.; Keenan, T.F.; Migliavacca, M.; Ryu, Y.; Sonnentag, O.; Toomey, M. Climate change, phenology, and phenological control of vegetation feedbacks to the climate system. *Agric. For. Meteorol.* **2013**, *169*, 156–173. [CrossRef]

32. Bhattacharjee, A.; Anadón, J.D.; Lohman, D.J.; Doleck, T.; Lakhankar, T.; Shrestha, B.B.; Thapa, P.; Devkota, D.; Tiwari, S.; Jha, A.; et al. The impact of climate change on biodiversity in Nepal: Current knowledge, lacunae, and opportunities. *Climate* **2017**, *5*, 80. [CrossRef]

33. Pliscoff, P.; Fuentes-Castillo, T. Representativeness of terrestrial ecosystems in Chile's protected area system. *Environ. Conserv.* **2011**, *38*, 303–311. [CrossRef]

34. Jaksic, F.M. Ecological effects of El Niño in terrestrial ecosystems of western South America. *Ecography* **2001**, *24*, 241–250. [CrossRef]

35. Squeo, F.A.; Loayza, A.P.; López, R.P.; Gutiérrez, J.R. Vegetation of Bosque Fray Jorge National Park and its surrounding matrix in the Coastal Desert of north-central Chile. *J. Arid Environ.* **2016**, *126*, 12–22. [CrossRef]

36. Holmgren, M.; Scheffer, M.; Ezcurra, E.; Gutiérrez, J.R.; Mohren, G.M. El Niño effects on the dynamics of terrestrial ecosystems. *Trends Ecol. Evol.* **2001**, *16*, 89–94. [CrossRef]

37. Garreaud, R.D.; Alvarez-Garreton, C.; Barichivich, J.; Boisier, J.P.; Christie, D.; Galleguillos, M.; LeQuesne, C.; McPhee, J.; Zambrano-Bigiarini, M. The 2010–2015 megadrought in central Chile: Impacts on regional hydroclimate and vegetation. *Hydrol. Earth Syst. Sci.* **2017**, *21*, 6307–6327. [CrossRef]

38. Úbeda, X.; Sarricolea, P. Wildfires in Chile: A review. *Glob. Planet Change* **2016**, *146*, 152–161. [CrossRef]

39. Urrutia-Jalabert, R.; González, M.E.; González-Reyes, Á.; Lara, A.; Garreaud, R. Climate variability and forest fires in central and south-central Chile. *Ecosphere* **2018**, *9*, e02171. [CrossRef]

40. Holz, A.; Paritsis, J.; Mundo, I.A.; Veblen, T.T.; Kitzberger, T.; Williamson, G.J.; Aráoz, E.; Bustos-Schindler, C.; González, M.E.; Grau, H.R.; et al. Southern Annular Mode drives multicentury wildfire activity in southern South America. *Proc. Natl. Acad. Sci. USA* **2017**, *114*, 9552–9557. [CrossRef]

41. Viale, M.; Garreaud, R. Orographic effects of the subtropical and extratropical Andes on upwind precipitating clouds. *J. Geophys. Res. Atmos.* **2015**, *120*, 4962–4974. [CrossRef]

42. Boisier, J.P.; Rondanelli, R.; Garreaud, R.D.; Muñoz, F. Anthropogenic and natural contributions to the Southeast Pacific precipitation decline and recent megadrought in central Chile. *Geophys. Res. Lett.* **2016**, *43*, 413–421. [CrossRef]

43. Quintana, J.; Aceituno, P. Changes in the rainfall regime along the extratropical west coast of South America (Chile): 30–43 ºS. *Atmósfera* **2012**, *25*, 1–22.

44. Alaniz, A.J. Chilean forest: Recent trends and perspectives. *Persp. Chall.* **2019**, 1–308.

45. Madariaga, G.C.; Navarro, R.C.; Baeza, Á.P.; Verrugio, G.C. Structural and biometric characterization of *Nothofagus betuloides* production forests in the Magellan Region, Chile. *J. Sustain. For.* **2007**, *24*, 123–140. [CrossRef]

46. Myers, N.; Mittermeier, R.A.; Mittermeier, C.G.; Da Fonseca, G.A.; Kent, J. Biodiversity hotspots for conservation priorities. *Nature* **2000**, *403*, 853. [CrossRef]

47. Díaz, I.A.; Armesto, J.J.; Reid, S.; Sieving, K.E.; Willson, M.F. Linking forest structure and composition: Avian diversity in successional forests of Chiloé Island, Chile. *Biol. Conserv.* **2005**, *123*, 91–101. [CrossRef]

48. Echeverría, C.; Newton, A.C.; Lara, A.; Benayas, J.M.R.; Coomes, D.A. Impacts of forest fragmentation on species composition and forest structure in the temperate landscape of Southern Chile. *Glob. Ecol. Biogeogr.* **2007**, *16*, 426–439. [CrossRef]

49. Petit, I.J.; Campoy, A.N.; Hevia, M.J.; Gaymer, C.F.; Squeo, F.A. Protected areas in Chile: Are we managing them? *Rev. Chil. Hist. Nat.* **2018**, *91*, 1. [CrossRef]

50. Jusys, T. Quantifying avoided deforestation in Pará: Protected areas, buffer zones and edge effects. *J. Nat. Conserv.* **2016**, *33*, 10–17. [CrossRef]

51. Núñez, J.; Rivera, D.; Oyarzún, R.; Arumí, J. Influence of Pacific Ocean multidecadal variability on the distributional properties of hydrological variables in north-central Chile. *J. Hydrol.* **2013**, *501*, 227–240. [CrossRef]

52. Saldías, G.S.; Largier, J.L.; Mendes, R.; Pérez-Santos, I.; Vargas, C.A.; Sobarzo, M. Satellite-measured interannual variability of turbid river plumes off central-southern Chile: Spatial patterns and the influence of climate variability. *Prog. Oceanogr.* **2016**, *146*, 212–222. [CrossRef]

53. Cazelles, B. Symbolic dynamics for identifying similarity between rhythms of ecological time series. *Ecol. Lett.* **2004**, *7*, 755–763. [CrossRef]

54. Cazelles, B.; Chavez, M.; Magny, G.C.d.; Guégan, J.F.; Hales, S. Time-dependent spectral analysis of epidemiological time-series with wavelets. *J. R. Soc. Interface* **2007**, *4*, 625–636. [CrossRef] [PubMed]

55. Chatfield, C.; Xing, H. *The Analysis of Time Series: An Introduction with R*; CRC Press, Taylor & Francis Group: Boca Raton, FL, USA, 2019.

56. Cazelles, B.; Chavez, M.; Berteaux, D.; Ménard, F.; Vik, J.O.; Jenouvrier, S.; Stenseth, N.C. Wavelet analysis of ecological time series. *Oecologia* **2008**, *156*, 287–304. [CrossRef]

57. Cazelles, B.; Cazelles, K.; Chavez, M. Wavelet analysis in ecology and epidemiology: Impact of statistical tests. *J. R. Soc. Interface* **2014**, *11*, 20130585. [CrossRef]

58. Morisette, J.T.; Richardson, A.D.; Knapp, A.K.; Fisher, J.I.; Graham, E.A.; Abatzoglou, J.; Wilson, B.E.; Breshears, D.D.; Henebry, G.M.; Hanes, J.M.; et al. Tracking the rhythm of the seasons in the face of global change: Phenological research in the 21st century. *Front. Ecol. Environ.* **2009**, *7*, 253–260. [CrossRef]

59. Taig-Johnston, M.; Strom, M.K.; Calhoun, K.; Nowak, K.; Ebensperger, L.A.; Hayes, L. The ecological value of long-term studies of birds and mammals in Central America, South America and Antarctica. *Rev. Chil. Hist. Nat.* **2017**, *90*, 1–13. [CrossRef]

60. Buermann, W.; Anderson, B.; Tucker, C.J.; Dickinson, R.E.; Lucht, W.; Potter, C.S.; Myneni, R.B. Interannual covariability in Northern Hemisphere air temperatures and greenness associated with El Niño-Southern Oscillation and the Arctic Oscillation. *J. Geophys. Res. Atmos.* **2003**, *108*. [CrossRef]

61. Trenberth, K.E.; Dai, A.; Van Der Schrier, G.; Jones, P.D.; Barichivich, J.; Briffa, K.R.; Sheffield, J. Global warming and changes in drought. *Nat. Clim. Chang.* **2014**, *4*, 17–22. [CrossRef]

62. Chen, W.; Feng, J.; Wu, R. Roles of ENSO and PDO in the link of the East Asian winter monsoon to the following summer monsoon. *J. Clim.* **2013**, *26*, 622–635. [CrossRef]

63. Schneider, W.; Donoso, D.; Garcés-Vargas, J.; Escribano, R. Water-column cooling and sea surface salinity increase in the upwelling region off central-south Chile driven by a poleward displacement of the South Pacific High. *Prog. Oceanogr.* **2017**, *151*, 38–48. [CrossRef]

64. Garreaud, R.D.; Boisier, J.P.; Rondanelli, R.; Montecinos, A.; Sepúlveda, H.H.; Veloso-Aguila, D. The central Chile mega drought (2010–2018): A climate dynamics perspective. *Int. J. Climatol.* **2020**, *40*, 421–439. [CrossRef]

65. McWethy, D.B.; Pauchard, A.; García, R.A.; Holz, A.; González, M.E.; Veblen, T.T.; Stahl, J.; Currey, B. Landscape drivers of recent fire activity (2001–2017) in south-central Chile. *PLoS ONE* **2018**, *13*, e0201195. [CrossRef]

66. Lara, C.; Cazelles, B.; Saldías, G.S.; Flores, R.P.; Paredes, Á.L.; Broitman, B.R. Coupled Biospheric Synchrony of the Coastal Temperate Ecosystem in Northern Patagonia: A Remote Sensing Analysis. *Remote Sens.* **2019**, *11*, 2092. [CrossRef]

67. Hessl, A.; Allen, K.J.; Vance, T.; Abram, N.J.; Saunders, K.M. Reconstructions of the southern annular mode (SAM) during the last millennium. *Prog. Phys. Geogr.* **2017**, *41*, 834–849. [CrossRef]

68. Marshall, G.J. Trends in the Southern Annular Mode from observations and reanalyses. *J. Clim.* **2003**, *16*, 4134–4143. [CrossRef]

69. Gong, D.; Wang, S. Definition of Antarctic oscillation index. *Geophys. Res. Lett.* **1999**, *26*, 459–462. [CrossRef]

70. Garreaud, R. Record-breaking climate anomalies lead to severe drought and environmental disruption in western Patagonia in 2016. *Clim. Res.* **2018**, *74*, 217–229. [CrossRef]

71. Wu, X.; Mao, J. Interdecadal modulation of ENSO-related spring rainfall over South China by the Pacific Decadal Oscillation. *Clim. Dyn.* **2016**, *47*, 3203–3220. [CrossRef]

72. Schoennagel, T.; Veblen, T.T.; Romme, W.H.; Sibold, J.S.; Cook, E.R. ENSO and PDO variability affect drought-induced fire occurrence in Rocky Mountain subalpine forests. *Ecol. Appl.* **2005**, *15*, 2000–2014. [CrossRef]

73. Wu, D.; Zhao, X.; Liang, S.; Zhou, T.; Huang, K.; Tang, B.; Zhao, W. Time-lag effects of global vegetation responses to climate change. *Glob. Chang. Biol.* **2015**, *21*, 3520–3531. [CrossRef]

74. Gutierrez, J.R.; Meserve, P.L.; Kelt, D.A.; Engilis Jr, A.; Previtali, M.A.; Milstead, W.B.; Jaksic, F.M. Long-term research in Bosque Fray Jorge National Park: Twenty years studying the role of biotic and abiotic factors in a Chilean semiarid scrubland. *Rev. Chil. Hist. Nat.* **2010**, *83*, 69–98. [CrossRef]

75. Meserve, P.L.; Kelt, D.A.; Previtali, M.A.; Milstead, W.B.; Gutiérrez, J.R. Global climate change and small mammal populations in north-central Chile. *J. Mammal.* **2011**, *92*, 1223–1235. [CrossRef]

76. Meserve, P.L.; Kelt, D.A.; Gutiérrez, J.R.; Previtali, M.A.; Milstead, W.B. Biotic interactions and community dynamics in the semiarid thorn scrub of Bosque Fray Jorge National Park, north-central Chile: A paradigm revisited. *J. Arid Environ.* **2016**, *126*, 81–88. [CrossRef]

77. Le Maire, G.; Marsden, C.; Nouvellon, Y.; Grinand, C.; Hakamada, R.; Stape, J.L.; Laclau, J.P. MODIS NDVI time-series allow the monitoring of Eucalyptus plantation biomass. *Remote Sens. Environ.* **2011**, *115*, 2613–2625. [CrossRef]

78. Huete, A.; Didan, K.; Miura, T.; Rodriguez, E.P.; Gao, X.; Ferreira, L.G. Overview of the radiometric and biophysical performance of the MODIS vegetation indices. *Remote Sens. Environ.* **2002**, *83*, 195–213. [CrossRef]

79. Lara, C.; Saldías, G.S.; Paredes, A.L.; Cazelles, B.; Broitman, B.R. Temporal variability of MODIS phenological indices in the temperate rainforest of Northern Patagonia. *Remote Sens.* **2018**, *10*, 956. [CrossRef]

80. Mutanga, O.; Skidmore, A.K. Narrow band vegetation indices overcome the saturation problem in biomass estimation. *Int. J. Remote Sens.* **2004**, *25*, 3999–4014. [CrossRef]